Experiments in Fluids 12, 173–180 (1992)

Experiments in Fluids

The influence of kinematic waves on jet break down

G. E. A. Meier *, A. Klöpper and **G. Grabitz**

Max-Planck-Institut für Strömungsforschung, 3400 Göttingen, Bunsenstr. 10, FRG

Abstract. The breakdown of a liquid jet is commonly considered as an effect of the surface tension. However, essential aspects of the boundary wave amplification and the final disintegration of velocity modulated jets can be explained by non-linear travelling time effects, which are of purely kinematic nature. The experiments are carried out on jets with radii between 1.2 to 2.5 mm and Weber numbers between 17 to 200. The experimental results are compared with a theoretical solution which neglects the surface tension.

1 Introduction

Travelling time effects which are the reason of many flow instabilities represent a very simple example of non-linear behaviour in flows, because they are based on purely kinematic conditions.

Liquid particles which start consecutively from a certain location with different velocities overtake (and surpass) each other after sufficient travelling times. This simple process induces a non-linear velocity field. The effects which result from this process are called travelling time effects [Grabitz and Meier (1983)]. Distorted liquid jets are analysed here as an example for these travelling time effects. They are easily produced by velocity modulation of the fluid in a nozzle. By means of one-dimensional depiction they can also be described theoretically.

Liquid jets were already successfully described by Lord Rayleigh (1878), while working on a stability theory. For infinitely small disturbances of the boundary of an infinitely long liquid column his calculations of the surface tension lead to growth rates of the disturbances and to stability criteria. Experimentally his results and those of Weber (1931) were confirmed by Haenlein (1931), Donaelly and Glaberson (1966), Goedde and Yuen (1970) and others. However, in those experiments, in which only a temporal disturbance is possible, the spatial growth rates were compared with the theoretical temporal growth rates. A justification for proceeding in this way was provided by Keller et al. (1973), who could prove that for large Weber numbers ($We \gg 1$; $We = \varrho RU^2/\sigma$; ϱ = density, R = jet radius; U = jet velocity, σ = surface tension), the modes of the temporal and spatial growth rate coincide. One-dimensional theories by Pimbley (1976) and Bogy (1978) calculated the amplification of velocity disturbances at the nozzle. For the growth they received identical results to those of Keller et al. (1973).

The occurrence of satellite droplets could not be explained by any of the above-mentioned theories. Using the methods of the perturbation theory the calculations were refined, e.g., by Yuen (1968) and Chaudhary and Redekopp (1980). They added terms of 2nd and 3rd order to the linear theory.

For very small disturbance amplitudes ε these non-linear theories proved to be in agreement with the experimental results. For somewhat greater amplitudes (already from $\varepsilon = 2\%$ onwards) there were discrepancies between the results and the theory.

This paper aims to show how the disturbance amplitude in this range ($\varepsilon > 2\%$) becomes dominant and how the non-linear travelling time effects get great influence on the jet disintegration. Grabitz and Meier (1983) have already referred to the significance of travelling time effects in some work with emphasis on the theoretical aspect. This work has introduced an exact solution of the non-linear Euler equation for the jet in one-dimensional form, neglecting the surface tension. This result is also used in this work, in comparison to the experiments.

The experiments are carried out on jets with a relatively large radius (1,5–2,5 mm). The large diameter jets enable the measurement of the velocity modulation directly with hot film probes in the jet and allow for a precise description of the disturbance-amplitude. For the generation of the velocity modulation a supply chamber was developed which provided the desired disturbance of the jet with a piston-mechanism. The piston's movement is controlled by a frequency generator which can vary the modulation in amplitude and frequency over wide ranges. The inlet chamber is designed in such a way that natural disturbances are reduced to a minimum.

* Present address: Institut für Experimentelle Strömungsmechanik, DLR, 3400 Göttingen, Bunsenstr. 10, FRG

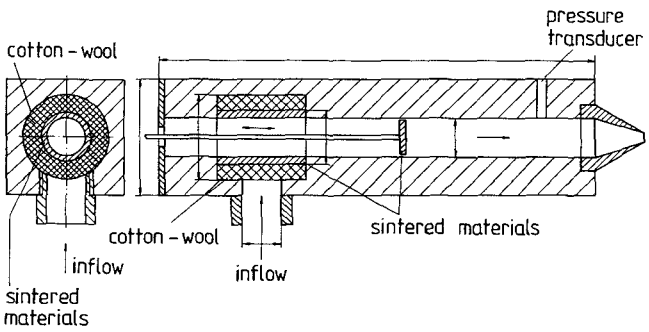

Fig. 1. Inlet chamber for the generation of velocity modulated jets in longitudinal- and cross-section

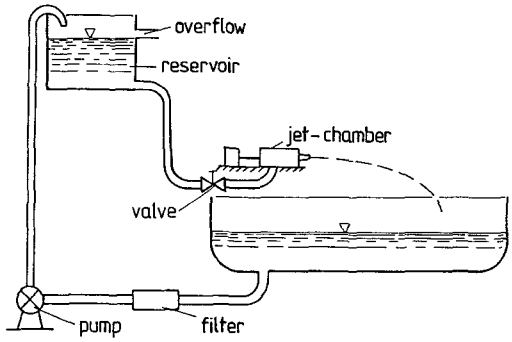

Fig. 2. Water circulation with supply container to generate constant pressure

2 Experimental set-up and parameters

To generate velocity modulated jets, the supply chamber shown in Fig. 1 is used. The liquid flows within the chamber through a porous piston (made of sintered material). The piston moves in the flow and induces a pressure and velocity fluctuation in the liquid. This causes the desired velocity modulation of the jet. The piston is moved by an electromagnetic vibrator which can be controlled by a sine wave generator with various frequencies and amplitudes.

The ring-shaped intake of the inlet chamber is lined with fiber material to avoid separations in the entering flow which could cause unwanted pressure fluctuations. Another purpose of the fiber felt is to generate a resistance as large as possible between the incoming flow and the nozzle flow. This was done to transmit the pressure oscillations of the piston mainly to the nozzle flow and to avoid pumping a major part of the energy into the hose. The inner side of the ring-shaped intake is covered by porous sintered material. This guarantees that the flow enters into the inlet chamber radially. Vortices are mostly avoided.

In the experiment radially symmetric nozzles with differently sized holes are used. The diameters of the apertures vary from 2.4–5.0 mm, but the inlet aperture has a constant diameter of 20 mm. Experience has shown that it is best to use long nozzles with a small inclination angle. Experiments with nozzles of different lengths have proved that the furthest reaching undisturbed jets originate from the longest nozzles. However a length of 5 cm has proved to be sufficient. In case of these smoothly converging nozzles the jet diameter equals the nozzle diameter within a few per cent.

The highly constant pressure in the intake of the nozzle flow is attained by a constant hydrostatic pressure of the liquid. The constant pressure is guaranteed by a stable height of the liquid level in the supply container (cf. Fig. 2) by means of an overflow outlet. The pressure of the intake flow can be set to any value by a regulating valve. This allows a variation of the jet velocities. Mechanical vibrations of the experimental set-up have been reduced to a sufficiently low level; in case of stronger vibrations induced by the pump and its engine the described phenomena are disturbed.

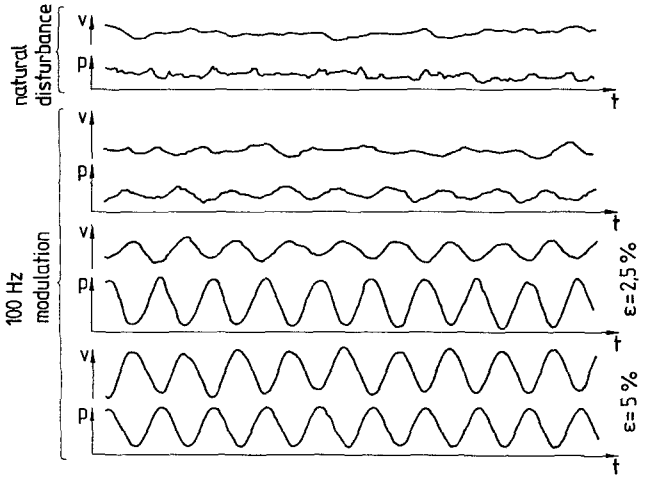

Fig. 3. Typical velocity and pressure signals, measured with a hot film probe and a pressure transducer with a mean jet velocity of $U = 2.0$ m/s. The diameter of the nozzle is 3 mm. The lower part of the figure shows pressure and velocity fluctuations where the flow is modulated by the piston at a frequency of 100 Hz and various amplitudes

The magnitude of the velocity fluctuations was determined by a hot film probe. The probe (length 1.5 mm, diameter 50 μm) was positioned in the jet a few millimeters downstream of the nozzle. Typical velocity and simultaneously measured pressure signals from the chamber are shown in Fig. 3. The velocity signals are very close to being sinusoidal and thus correspond almost exactly to the desired velocity modulation. Calibrating measurements were necessary to adjust the velocity modulation. The complete measuring set-up is shown in Fig. 4.

The correct velocity modulation was set in the following way: The amplitude of the piston movement at a certain frequency was adjusted with a frequency generator until the hot film probe registered the desired amplitude of the velocity fluctuation. Then the corresponding pressure amplitude in the inlet chamber was measured. In the following jet

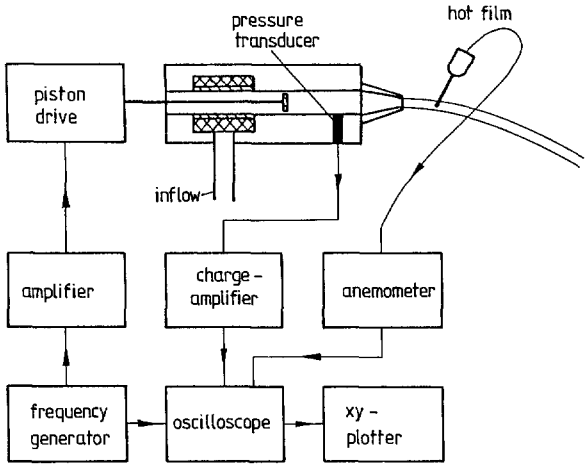

Fig. 4. Measurement set-up and measuring instruments to adjust and measure the velocity modulation

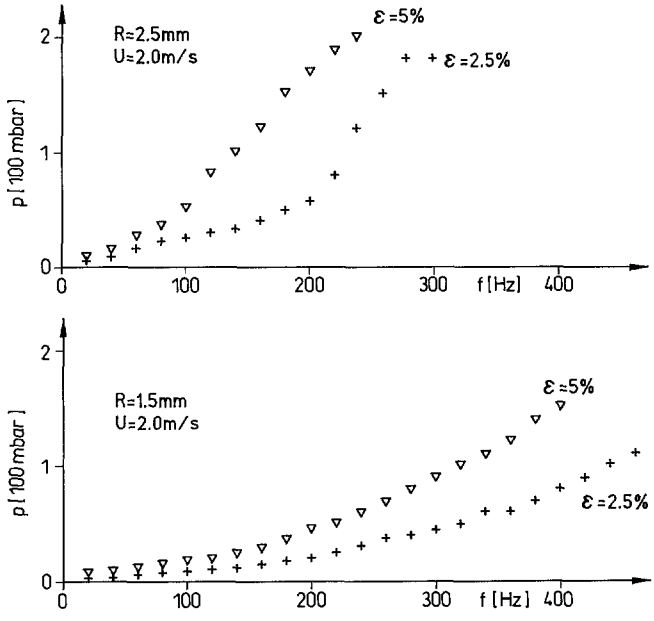

Fig. 5. Pressure frequency curves for constant velocity fluctuation of the nozzle aperture. The pressure amplitude for the respective frequency that was necessary to generate a certain velocity amplitude is plotted

experiments the probe would have been an obstruction and was removed from the jet. The pressure amplitude served as a reference to adjust the desired velocity modulation. A few of these calibrating curves are shown in Fig. 5. The curves show which pressure amplitudes at different frequencies are necessary to generate a velocity disturbance of 2.5 or 5%. To reach the same velocity amplitude one has to increase the pressure at high frequencies greatly. This increase limits the range of measurements that can be obtained with this apparatus.

For high frequencies the piston movement is limited in its performance. For the natural disturbance, i.e. unwanted disturbances that are caused by the apparatus, this great increase of the pressure amplitude means that disturbances of high frequency are damped strongly at the nozzle. Therefore the natural disturbance is limited to a range of low frequencies (<100 Hz). The magnitude of the disturbance for this frequency range is approximately at 0.5–0.7% of the respective basic velocity. This value is taken from the pressure measurements since the pressure transducer in contrast to the hot film probe still supplies reliable values in this range ($<1\%$).

The modulation function

$$w_a(t) = U(1+\varepsilon \sin(2\pi f t)) \tag{1}$$

contains the amplitude and the frequency as variable parameters. The frequency f is adjustable to any value even above 1 KHz. However, the velocity amplitude, as described above, strongly depends on the frequency. Therefore up to about 250–400 Hz (depending on the nozzle size) amplitudes up to 5% of the basic velocity can be reached. For smaller frequencies (<100 Hz) amplitudes up to 100% are possible.

For the droplet formation and the disintegration of liquid jets the Weber number

$$We = \frac{\varrho R_a U^2}{\sigma} \tag{2}$$

(ϱ = density, U = basic velocity, R_a = nozzle radius, σ = surface tension) is of great importance because of the influence of the surface tension. Since water is the only liquid used in the experiment, the only variable parameters remaining are the nozzle radius R and the basic velocity U. The nozzles used had radii between 1.2 and 2.5 mm, the jet velocities reached from 1.0 m/s to 3.0 m/s. The Weber number range covered by these values lies between 17 and 200.

3 Experiments

Differently modulated jets are examined at various Weber numbers. The jets are photographed and the edges are measured. The pictures are taken in 35 mm format using high-resolution film material. The jets are photographed in front of a white background which is illuminated evenly by four flash-lights. Another flash-light illuminates the jet from the front. Fig. 6 shows a picture series which was used for a quantitative analysis.

To show the influence of travelling time effects they will be explained qualitatively by means of the pictures in Fig. 7. Picture 7 a shows a jet with a very small modulation frequency. As an effect of gravitation the velocity modulation is very well perceptible: The jet's curvature modulation results from the liquid particles with different velocities flying along different parabolic paths. If the frequency is increased, as in Fig. 7 b, the time period is not large enough for gravitation to "pull apart" the particles. Because of the shorter time

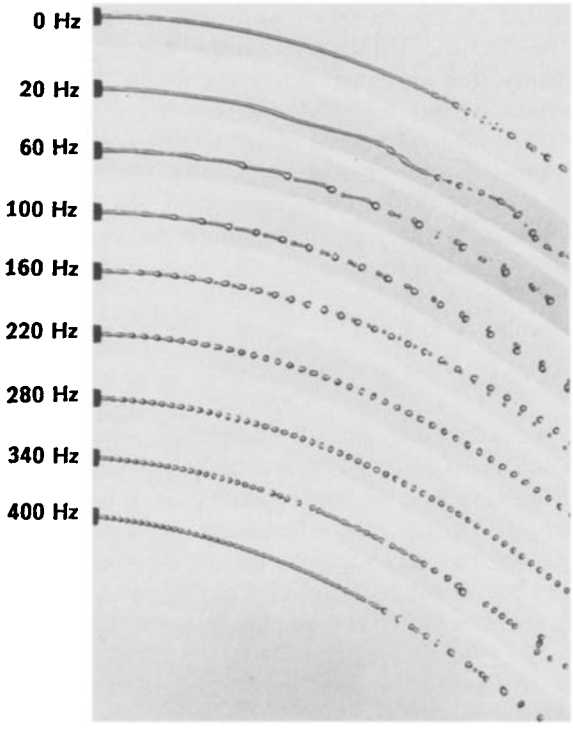

Fig. 6. Photos chosen as typical examples of the experiments. The top left picture depicts a jet without velocity modulation, the disintegration occurs only by natural disturbance. The other jets are stimulated at the frequency rate given on the photos. In the lower pictures the transition to stability is perceptible

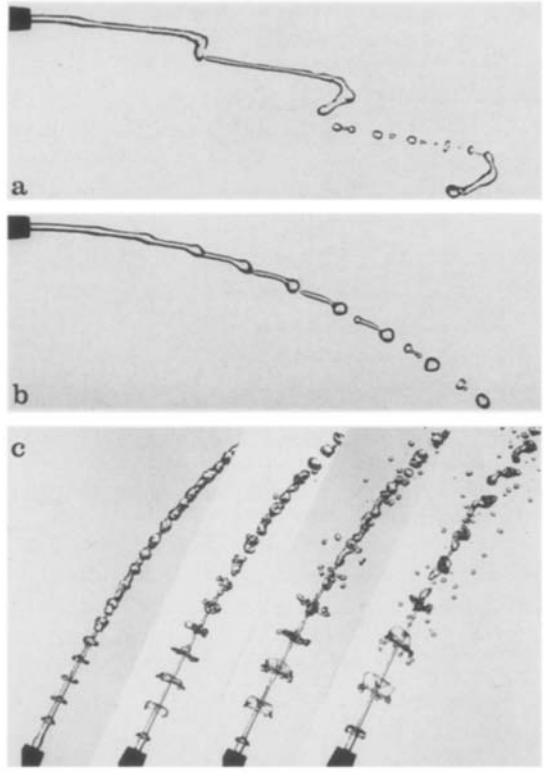

Fig. 7a–c. The influence of travelling time effects; **a** modulation frequency: 10 Hz, $\varepsilon = 5\%$; **b** modulation frequency: 50 Hz, $\varepsilon = 5\%$; **c** modulation with very large disturbance amplitudes $\varepsilon > 50\%$, at several frequencies

period, the particles of different velocity catch up with each other in a shorter time. The liquid particles hit upon each other and the jet becomes thicker at these points, as shown in the photo. In other places, where the fast particles were previously, the jet becomes thinner.

If the amplitude is also increased (as shown in Fig. 7c), the process of catching up takes place in a far shorter time because of the greater velocity differences. The particles now hit very rapidly and at such great number on each other, that the liquid material is pushed flat towards the outside. Figures 8 and 9 show the growth of the disturbance in greater detail. The jets originate from nozzles of 2, 4 and 5 mm diameter, respectively. Their velocity is modulated with disturbance amplitudes of 2.5 and 5%. Even for these jets with a relatively small disturbance, a separation of the liquid is clearly visible. Because of the velocity differences the liquid pushes forward and forms spherical clusters. Simultaneously thin connections remain between the clusters, growing thicker in the direction of motion.

This separation effect is clearly dependent on the amplitude and increases greatly for large disturbances, as shown in the first pictures. Because of this separation the jet's shape cannot be described by simple sine functions, connected with an exponential term for the growth. Additionally the clusters do not grow very much in diameter, whereas the thin connections steadily become thinner.

In addition to the influence of the travelling time effects, which cause the concentration of liquid in certain points, one has to consider the influence of the surface tension finally. The surface tension leads to the formation of drops, cutting off the thin connections in the jet. It also is the reason for the spherical shape of the clusters of liquid. Without surface tension, the drops would have a flat shape like in the jets with greater disturbance amplitudes.

The lower jets in the pictures 8 and 9 are very interesting. After a quite significant momentary growth, the jet becomes smoother and it stabilises. All those modulated jets that do not disintegrate due to the stimulating modulation are called stable. Within the linear stability theory however, a growth of the disturbance is not taken into account.

Stability limits have been determined quantitatively for four Weber numbers (17, 51, 90, 141) and two disturbance amplitudes (2.5 and 5%).

The following stability criteria were assumed:

1) The modulated jet should approximately reach the length of the natural disintegration, i.e. the disintegration length of an unmodulated jet.

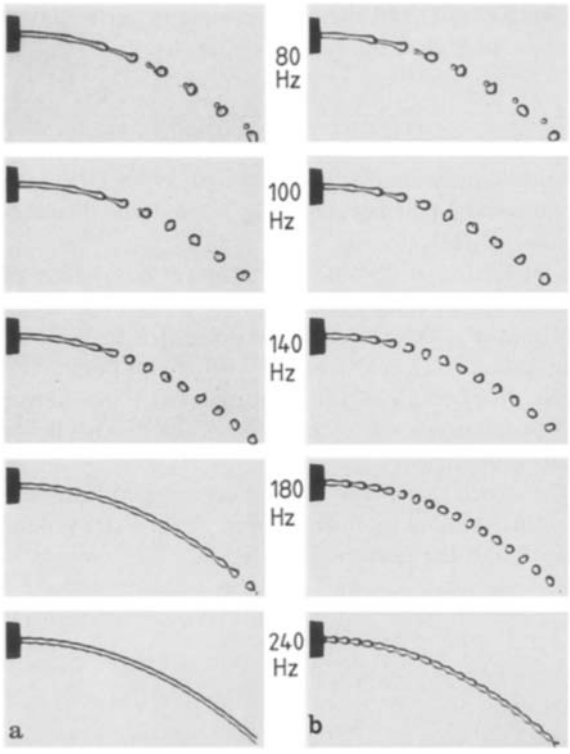

Fig. 8 a and b. Details of the jet's beginning for various modulation frequencies; from top to bottom: 80 Hz, 100 Hz, 140 Hz, 180 Hz, 240 Hz. The diameter of the nozzle is 2.4 mm, the mean jet velocity is $U=1.0$ m/s ($We=17$). The lower jets are both stable in relation to the frequency; **a** disturbance amplitude $\varepsilon=2.5\%$; **b** disturbance amplitude $\varepsilon=5.0\%$

2) The droplet sequence with which the jet disintegrates must not correspond to the stimulating frequency.

These criteria certify that the jet is stable in relation to the stimulating frequency. The transition to stability can be seen clearly in Fig. 9.

The measured results are shown in the stability diagram (Fig. 10) with the nondimensional frequency of the distortion plotted against the Weber number.

The frequency $2\pi f$ is made dimensionless with the nozzle radius R and the basic velocity U. The results show that the stability limit is dependent on the disturbance amplitude. The solid line in the diagram shows the stability limit following from the linear theory.

Apart from the stability diagram, the disintegration lengths for the Weber number 17, 51, 90 and 141, each one for two disturbance amplitudes (2.5 and 5%), were determined. The disintegration length is the length of the jet before disintegrating into drops. The lengths measured on the photographs are made dimensionless with the nozzle radius R and are plotted over the dimensionless disturbance frequency Ω, Fig. 11.

In spite of varying Weber numbers, the measured disintegration lengths hardly deviate from each other. The lengths rather depend on the disturbance amplitude and on the modulation frequency. With increasing frequency the disintegration length constantly decreases. The shape of the disintegration length's curve is similar to a hyperbola and does not show any significant minimum.

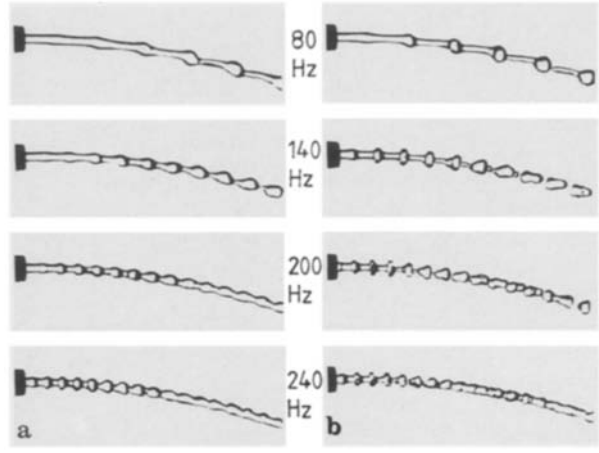

Fig. 9. a and b. Details of the beginning of the jet for various modulation frequencies; from top to bottom: 80 Hz, 140 Hz, 200 Hz, 240 Hz. The diameter of the nozzle is 5 mm, the mean jet velocity is $U=2.0$ m/s ($We=141$); **a** disturbance amplitude $\varepsilon=2.5\%$; **b** disturbance amplitude $\varepsilon=5.0\%$

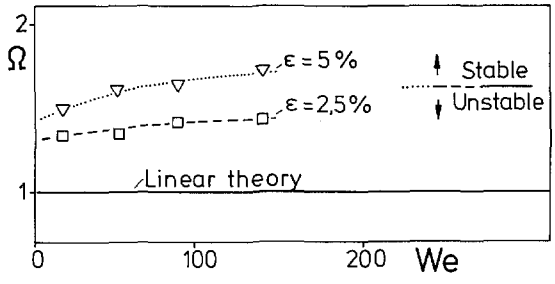

Fig. 10. Stability diagram for modulated liquid jets

4 Theoretical solution

We consider the incompressible fluid stream as an inviscid one-dimensional unsteady flow without surface tension. The pressure inside the jet is equal to the ambient pressure. Thus the flow is determined only by the velocity $w(x, t)$ and the cross-sectional area $F(x, t)$ of the jet. The symbols t and x denote the time and space co-ordinates in the flow direction, respectively. The symbol γ means $\pm g$ or zero according to the orientation of the jet in the gravitational field (g is the gravity acceleration).

The conservation equations of mass and momentum are

$$\frac{\partial F}{\partial t}+w\frac{\partial F}{\partial x}+F\frac{\partial w}{\partial x}=0 \tag{3}$$

$$\frac{\partial w}{\partial t}+w\frac{\partial w}{\partial x}=\gamma \tag{4}$$

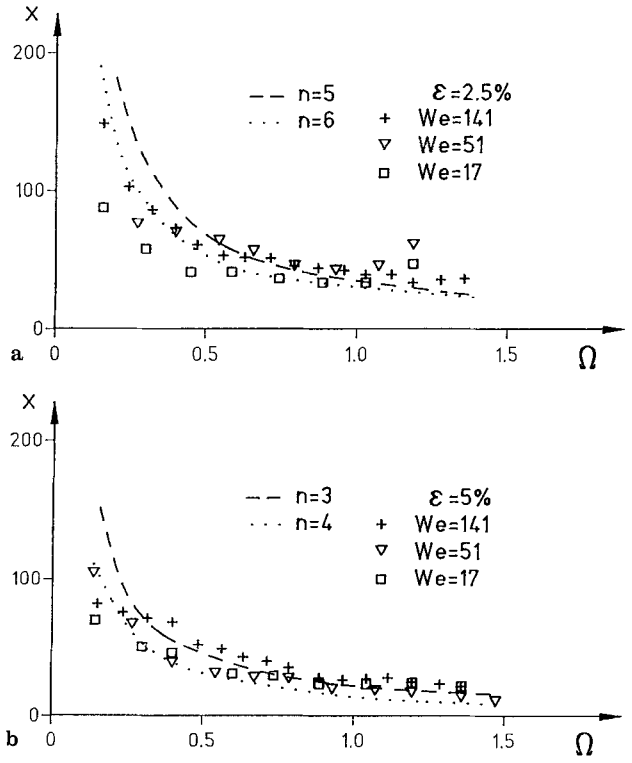

Fig. 11 a and b. Measured dimensionless disintegration lengths x for all three Weber numbers and fitted caves following Eq. (20); **a** disturbance amplitude $\varepsilon = 2.5\%$; **b** disturbance amplitude $\varepsilon = 5.0\%$

and the boundary conditions at $x=0$ are

$$w(0,t) = w_a(t) \tag{5}$$

$$F(0,t) = F_a(t)\,. \tag{6}$$

We introduce Lagrange co-ordinates by the following transform:

$$t(\vartheta,\tau) = \vartheta \tag{7}$$

$$x(\vartheta,\tau) = w_a(\tau)\,(\vartheta-\tau) + \frac{\gamma}{2}(\vartheta-\tau)^2 \tag{8}$$

The co-ordinate ϑ stands for the actual time and τ means the starting time of the flow particles.

With the help of this transform one arrives at the following solution [Grabitz and Meier (1983)] for the velocity w and the cross-section F:

$$w(\vartheta,\tau) = w_a(\tau) + \gamma(\vartheta-\tau)\,. \tag{9}$$

$$F(\vartheta,\tau) = \frac{F_a(\tau)\,w_a(\tau)}{\left|w_a(\tau) - (\vartheta-\tau)\left[\dfrac{\mathrm{d}w_a(\tau)}{\mathrm{d}t} - \gamma\right]\right|} \tag{10}$$

For comparison with our experiments we consider the special case of an axisymmetric jet which originates in a nozzle of constant radius R_a with a perturbed velocity of the form

$$w_a(\tau) = U[1 + \varepsilon \sin(\omega\tau)] \tag{11}$$

with the frequency ω and the relative velocity perturbation ε. Then the radius R of the jet is given as

$$\frac{R(\hat{\vartheta},\hat{\tau})}{R_a} = \sqrt{\left|\frac{1+\varepsilon\sin(\Omega\hat{\tau})}{1+\varepsilon\sin(\Omega\hat{\tau}) + [G-\varepsilon\Omega\cos(\Omega\hat{\tau})](\hat{\vartheta}-\hat{\tau})}\right|} \tag{12}$$

with the non-dimensional times $\hat{\vartheta} = \vartheta U/R_a$, $\hat{\tau} = \tau U/R_a$, the non-dimensional frequency $\Omega = \omega R_a/U$, and the Froude-number $G = \gamma R_a/U^2$.

If the distortion is $\varepsilon > G/\Omega$, the solution has points of infinite radius. Beginning with the position $x=0$ (i.e. $\hat{\vartheta}=\hat{\tau}$), points of maximal cross-section are generated in periodic travelling distances. Downstream of the first point of infinite radius, the distribution of the flow material is no longer unique. For the case $\varepsilon < G/\Omega$ damping of the distortions of the stream is predicted.

For the special case $G=0$ (no acceleration) with the Eqs. (5)–(10) the following much simpler result is derived for the radius R and the peak position x_p:

$$\frac{R}{R_a} = \sqrt{\left|\frac{x_p(\hat{\tau})}{x_p(\hat{\tau}) - x}\right|} \tag{13}$$

with

$$\frac{x_p(\hat{\tau})}{R_a} = \frac{[1+\varepsilon\sin(\Omega\hat{\tau})]^2}{\varepsilon\Omega\cos(\Omega\hat{\tau})} \tag{14}$$

The starting time τ of a liquid element determines whether there is a positive finite position x_p where the radius becomes infinite. In contrast to the linear stability theory, where exponential growth of the amplitude is typical, in this exact solution of the non-linear equation of motion the maximum radius goes to infinity like $(x_p - x)^{-1/2}$ for $(x_p - x) \to 0$. For the two-dimensional case, corresponding to flow in a channel or duct, the deflection of the interface between the distorted and the undistorted stream is

$$\frac{h}{h_a} = \left|\frac{x_p(\hat{\tau})}{x_p(\hat{\tau}) - x}\right| \tag{15}$$

In this case the amplification of the wave ridges of the interface goes with $(x_p - x)^{-1}$ for $(x_p - x)$ approaching 0. This means that in two dimensions the amplitudes go faster towards infinity than in the case of rotational symmetry.

5 Interpretation and discussion

We will now directly compare the experimental results with the solution of the one-dimensional travelling time theory. Jet pictures of the experiments will be directly compared to calculated jet paths, following Eq. (12), cf. Fig. 12. As can be seen, the experimental results are in agreement with the theoretical prediction. While the shape of the calculated jet edge in some places deviates from the photographed jets, especially in the peaks occurring later on, the mass concentration is described correctly. The mass distribution, i.e. the

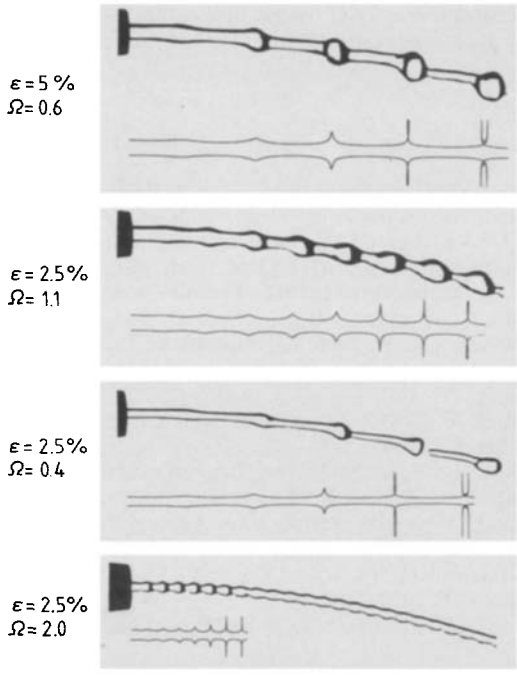

Fig. 12. Comparison of the experimental jets to jets calculated with the travelling time theory

clustering of the flow material and the formation of thin connections is already explicable by the travelling time. While the first section of the jets coincide very well with the theory, later on the shape deviates a little from the calculated one.

In this distant section the surface tension, that had been completely neglected in the theory, becomes effective. The tension does not allow the peaks that theoretically should appear. It forms the clusters to spherical masses. In this section the mass distribution is not only a result of the travelling time effects. The dynamics of the surface tension amplify or reduce the tendency of some liquid particles to propagate. The different curvature radii in the clusters and thin connections cause pressure differences between the thinner and thicker sections of the jet. In the case of two clusters being far apart from each other, low pressure develops in the clusters in relation to higher pressure in the connecting jet sections. As a consequence, the liquid is sucked into the clusters and more and more liquid particles collide. This can be seen in the top three jets of Fig. 12. In the lower jet, where two clusters lie very close to each other, the influence of the surface tension causes an opposite reaction. In this case an area of low pressure develops in the thin parts of the jet. The deformation caused by the travelling time effect is thus reversed by the effect of surface tension. This varying effect of the surface tension is caused by the varying ratio of the main curvature radius that describes the pressure of the surface tension in the jet in the following way, cf. Prandtl et al. (1984):

$$p=\sigma\left(\frac{1}{R_1}+\frac{1}{R_2}\right) \tag{16}$$

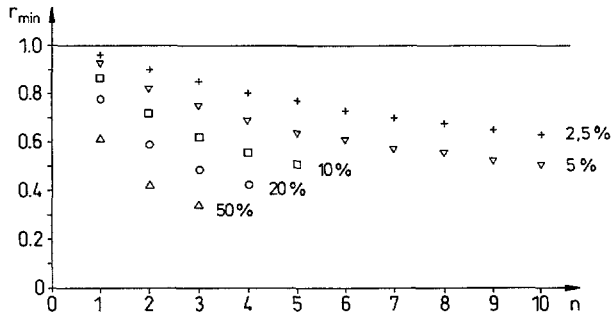

Fig. 13. Sizes of the jet mimima of the dimensionless jet radius calculated with the travelling time theory for various disturbance amplitudes

R_1 and R_2 are the radial and tangential curvature radii in the jet. The final formation of drops also results from this fact with the jet's connection being tied off. By comparing the jets with the theory, one sees that the cause of the clustering in the jet are the travelling time effects. The initial jet shape follows from the velocity discrepancies of the liquid particles. In the later stages of the jet, an interaction of the surface tension occurs. It becomes more and more dominant until the jets disintegrate into drops.

As the comparison of the theory to the experiment shows, the travelling time effect causes a significant deformation of the jet and thus a strong growth of the disturbance. The best agreement between the theory and the experiments is achieved in the thin sections of the jet, the jet minima. Thus these minima are used here to determine the growth of the disturbance quantitatively, using the travelling time theory. In this theory the jet in these sections gets the radius

$$R_{\min}=\sqrt{\frac{1}{(2n-1)\,\pi\varepsilon+1}} \tag{17}$$

This formula results from inserting the times for the minima

$$\tau_{\min}=-\frac{(2n-1)\,\pi}{\Omega} \tag{18}$$

Here n is a natural number and represents the number of periods. The size of the jet minima are shown in Fig. 13. The curves show the decrease of the jet radii in the minima for various disturbance amplitudes. It is noticeable that the radius for little disturbances already decreases after only a few periods. For reasons of continuity an increase in other parts should be expected. The locations of the minima result from the following relationship, which was worked out by transforming back the co-ordinate equation:

$$x=(1+\varepsilon\sin(\Omega\tau))\frac{(2n-1)\,\pi}{\Omega} \tag{19}$$

For small ε we can write

$$x=\frac{(2n-1)\,\pi}{\Omega} \tag{20}$$

This resembles an hyperbola, dependent on Ω, if n is kept constant. Since the disintegration lengths measured during disintegration had a hyperbolic shape, too, it was tried to fit the measured values to this relation. In doing this, the number n has to be adapted correctly. As shown in Fig. 11, this can be done very well. The number n shows in the diagrams of Fig. 11 that in terms of the period length, the disintegration length mainly is a function of the amplitude of the velocity distortion.

6 Conclusion

Stability experiments have been carried out on water jets with radii between 1.2 and 2.5 mm and Weber numbers between 17 and 200. A special distortion mechanism has produced modulations which are very close to being sinusoidal while both the amplitude and the frequency were well defined.

Photographic pictures of the decomposing jets were compared with the authors' kinematic wave theory which neglects the surface tension. Thus it can be shown that for Weber numbers of the order $We > 10$ the wave amplification and final disintegration of the velocity modulated jets are strongly influenced by non-linear travelling time effects. A stability diagram is given which also shows the influence by the amplitude of the velocity distortion on the stability.

In the case of low frequencies both the travelling time effect and the surface tension amplify the disintegration of the jet. But in the case of higher frequencies the surface tension causes a damping of the surface waviness and one observes an interesting phenomenon: after a quite significant growth just behind the nozzle, the jet downstream becomes smoother and gets stabilised.

References

Bogy, D. B. 1978: Use of one-dimensional Cosserat theory to study instability in a viscous liquid jet. Phys. Fluids 21, 190–197

Chaudhary, K. G.; Redekopp, L. G. 1980: The nonlinear capillary instability of a liquid jet (part 1). J. Fluid Mech. 96, 257–274

Chaudhary, K. G.; Maxworthy, T. 1980: The nonlinear capillary instability of a liquid jet (part 2). J. Fluid Mech. 96, 275–297

Donelly, R. J.; Glaberson, W. 1966: Experiments on the capillary instability of a liquid jet. Proc. Roy. Soc. London A 290, 547–556

Goedde, E. F.; Yuen, M. G. 1970: Experiments on liquid jets instability. J. Fluid Mech. 40, 495–511

Grabitz, G.; Meier, G. E. A. 1983: Über Laufzeitinstabilitäten in Flüssigkeitsstrahlen. Zamm 63, T 255–257

Haenlein, A. 1931: Über den Zerfall eines Flüssigkeitsstrahles. Forschung 2, 4, 139–148

Keller, J. B.; Rubinow, S. I.; Tu, Y. D. 1973: Spatial instability of a jet. Phys. Fluids 16, 2052–2055

Rayleigh, Lord 1878: On the instability of jets. Proc. London Math. Soc. X.

Pimbley, W. T. 1976: Drop formation from a liquid jet: A linear one-dimensional analysis considered as a boundary value problem. IBM J. Res. Develop, 148–156

Prandtl, L.; Oswatitsch, K.; Wieghardt, K. 1984: Führer durch die Strömungslehre, 8. Auflage. Braunschweig, p. 24

Weber, G. 1931: Zum Zerfall eines Flüssigkeitsstrahles. ZAMM 11, 136–154

Yuen, M.-C. 1968: Non-linear capillary instability of a liquid jet. J. Fluid Mech. 33, 151–163

Received January 29, 1991